J Mater Sci (2007) 42:4916–4925
DOI 10.1007/s10853-006-0397-9

Macromolecule-metal complexes ultrathin brushes with nanoscale protrusions grown from self-assembled monolayer by ATRP

Ke Sha · Dong Shuang Li · Yapeng Li · Shuwei Wang · Jingyuan Wang

Received: 3 December 2004 / Accepted: 2 May 2006 / Published online: 9 March 2007

Abstract Homopolymer and macromolecule-metal complexes (MMC) brushes on silicon wafers were successfully synthesized by the combination of self-assembly of the monolayer of initiator, atom transfer radical polymerization (ATRP) and coordination to metal ions. The initiator monolayer attached to silicon wafers was prepared by self-assembly of 3-aminopropyltriethoxysilane followed by amidation with α-bromopropionyl bromide, and permitted subsequent surface-initiated ATRP of butyl methacrylate (BMA) and acrylamide (AAM). From atomic force microscope (AFM) images it could be observed that the surface of poly(butyl methacrylate) (PBMA) brushes was uniform, while the surface of polyacrylamide (PAAM) brushes grew a large number of nanoscale protrusions. After coordination to metal ions, Pb^{2+} and Cd^{2+}, MMC brushes of PAAM were formed, while the nanoprotrusions with different sizes and densities were observed on the surface of MMC brushes. X-ray photoelectron spectroscopy (XPS) was used to determine a molar ratio of 2.80C:1.00O: 0.75N for the PAAM brushes, in good agreement with the value (3.00C:1.00O:1.00N) based on the monomer AAM. Moreover, the occurrence of the new XPS signals of metal ions Pb^{2+} (139.1 and 143.8 eV) and Cd^{2+} (405.4 and 412.5 eV) verified the formation of the MMC brushes.

K. Sha · D. S. Li · Y. Li · S. Wang · J. Wang (✉)
Alan G. MacDiarmid Institute of Jilin University, Changchun 130023, P.R. China
e-mail: jingyuanwang_jlu@yahoo.com.cn

Introduction

Tethering of polymer brushes on a solid substrate is an effective method of modifying the surface properties of the substrate [1, 2]. Considerable attention has been paid to the manipulation and control of the surface properties of solid substrate [3]. Polymer chains with a sufficiently high grafting density tethered to a surface or interface are of increasingly importance because of their distinctive chemical and physical properties, such as low intrinsic viscosity, high solubility, good miscibility, and polyfunctionality [4]. Based on these intrinsic properties, polymer brushes attached to flat substrate surfaces are useful in many applications, including data storage, nanolithography, corrosion inhibition, chemical sensing, cellular engineering, surface passivation, and micrometer-scale patterning [5–7].

The progresses in polymerization methods enable the preparation of well-defined graft polymer chains on various substrate surfaces by controlled/living radical polymerization such as nitroxide-mediated radical polymerization [8, 9], reversible addition-fragmentation chain transfer polymerization [10], and atom transfer radical polymerization (ATRP) [11–13]. This is due to their advantages, i.e., the film thickness is controlled and adjustable and the film properties can be finely accommodated by introducing a variety of functional groups or by copolymerization [14], which will make the materials diversification and functionality. In living/controlled radical polymerization methods we have known well, ATRP is the most versatile [15, 16] due to being suitable for most of functional styrenic and (meth)acrylate monomers; at the same time, its reaction condition is also modest and only requires the

absence of oxygen, the reaction is tolerant to water, and occurs in a conventional temperature range from the room temperature to 130 °C. In addition, ATRP has been used for modifying the surface properties of various substrates [11–13]. A successful ATRP is accomplished by fast initiation and more rapid reversible deactivation, which can keep a low concentration of the active species R· during the course of reaction, leading to not only a small contribution to termination but also a uniform growth of all the chains. A general mechanism for ATRP is shown in Scheme 1.

Macromolecule-metal complexes (MMC) play an essential role in biological fields and chemical industries, wherein metal ions can be bound to the polymer ligand by a coordinate bond [17]. Owing to the combination of the properties of organic polymer and those of metal ions, MMC has their potential application in environmental chemistry, and they are used as high efficient catalysts, electrochemical materials, optimized sensory, and especially as models for enzymes [18–20]. When MMC is employed in the surface modification of solid substrates, MMC brushes with thickness in molecular dimensions can alter the chemical and electrical interface characteristics of the underlying substrates and provide new pathways to functionalize surface for the potential application such as sensory devices. In addition, high efficient MMC catalyst attached to solid substrate (e.g. silicon wafer, spherical silicon gel, etc.) will also benefit its recycle.

The synthesis of MMC brushes refers to two consecutive processes: the attachment of the homopolymer (or copolymer) chains containing the coordination groups onto solid substrates and then coordination to metal ions. Commonly, the grafted polymers are prepared by interaction between end-functionalized (co)polymers and functional groups bonded to the substrates; however, this technique has a limited grafted density because of the fact that further grafting is hindered by the polymer chains already adsorbed on the surface [21]. An alternative technique has been successful use of surface-initiated polymerization [8–13] to modify surfaces of solid substrates. Due to the suitability for most of the functional (meth)acrylate and styrenic monomer, the coordination groups containing anchoring sites like nitrogen or oxygen are easy to be introduced into the polymer brushes by means of

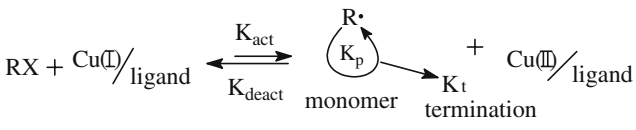

Scheme 1 A general mechanism of ATRP

ATRP technique [22]. Thus, the preparation of MMC brushes attached to solid substrates can be carried out by the integration of surface-initiated ATRP and coordination to metal ions.

In this work, homopolymer brushes of BMA and AAM were prepared by the combination of the self-assembly of initiator and ATRP technique, respectively. A uniform PBMA brushes was prepared, however, a lot of nanoscale protrusions appeared on the surface of PAAM brushes. After coordination to the metal ions, Pb^{2+} and Cd^{2+}, MMC brushes of PAAM were synthesized, the brushes grew nanoscale MMC protrusions whose size was larger than PAAM nanoprotrusions prior to coordination. The resulting polymer brushes were analyzed by means of XPS, AFM, UV-visible spectrum and contact angle measurement.

Experimental section

Chemicals

N,*N*-Dimethylformamide (DMF, 99%, Beijing chemical Co.) was distilled under vacuum having been dried with NaOH. Copper(I) chloride (CuCl, 97%, Beijing Chemical Co.) was purified by precipitation from acetic acid to remove Cu^{2+}, filtrated and washed with ethanol and then dried. Acrylamide (99%, Beijing Chemical Co.) was recrystallized from acetone. Butyl methacrylate (97%, Beijing Chemical Co.) was dried with CaH_2 and distilled under vacuum. 2,2′-Bipyridine (97%, Beijing Chemical Co.), α-bromopropionyl bromide (97%, Fluka Chemical Co.), DL-ethyl-bromopropionate (97%, Acros Chemical Co.), 3-aminopropyltriethoxysilane (99%, Aldrich Chemical Co.), Lead(II) acetate trihydrate ($Pb(CH_3COO)_2 3H_2O$, 97%, Beijing Chemical Co.), Cadmium(II) acetate dihydrate ($Cd(CH_3COO)_2 2H_2O$, 97%, Beijing Chemical Co.) were used without further purification. Toluene (99%, Tianjin Chemical Co.) was washed by concentrated H_2SO_4, H_2O, a 10% Na_2CO_3 solution, H_2O in turn and then dried with CaH_2, distilled. Triethylamine (99%, Beijing Chemical Co.) was refluxed for12 h in the presence of CaH_2 and distilled under vacuum.

Substrate treatment

The silicon wafers were ultrasonically cleaned for 5 min in succession with toluene, acetone, ethanol and water. Having been cleaned, the wafers were etched with a hydrofluoric acid solution (10%) for about 2 min and then rinsed with a large amount of water.

The silicon wafers were put into a bath containing the solution of concentrated H_2SO_4:H_2O_2 (v/v 5:5) at 60 °C for several hours, and then washed thoroughly with water. The contact angle of water on the wafers was 15°, revealing the cleanness and the uniformity of the surface. Subsequently, self-assembly was carried out on the silicon wafers.

Monolayer self-assembly and initiator synthesis

The above-modified wafers were put into a solution of 3-aminopropyltriethoxysilane (9.46×10^{-2} g, 4.27×10^{-4} mol) in dry toluene (5×10^{-6} m^3) for 18 h without stirring at room temperature. The wafers were cleaned under ultrasonic treatment in dry toluene and absolute ethanol for 5 min, respectively. The wafers were dried in a nitrogen (N_2) stream.

The silicon wafers with the layer of 3-aminopropyltriethoxysilane were immersed into a bath of triethylamine (7.25×10^{-2} g, 7.16×10^{-4} mol) in dry toluene (5×10^{-6} m^3) and then cooled in an ice bath (0 °C). After 10 min, α-bromopropionyl bromide (0.1 g, 4.77×10^{-4} mol) was added dropwise to it. The reaction was carried out at 0 °C for 2 h and then at room temperature for 5 h (Scheme 2). The color of the solution changed from white to yellow. The wafers were rinsed with toluene and absolute ethanol, respectively, and then dried in a N_2 stream. The silicon wafers with the initiator monolayer were either used immediately for polymerization or stored in a dry box at room temperature.

The synthesis of PAAM brushes on silicon wafers

The wafers with the initiator monolayer including the α-bromoester groups were immersed into 1×10^{-5} m^3 of a DMF solution of 1.422 g (2×10^{-2} mol) of acrylamide and 0.014 g (8.96×10^{-5} mol) of 2,2′-bipyridine, the mixture solution was bubbled with N_2 for 10 min, and then 0.004 g (4×10^{-5} mol) of CuCl was put into the mixture. The reaction continued under a N_2 stream and was heated in an oil bath at 120 °C for several hours. Throughout the reaction the color kept maroon (Scheme 2). After the polymerization, the wafers were ultrasonically cleaned for 5 min in a DMF solution and rinsed with a large amount of ultrapure water. The wafers were immersed into ultrapure water for 24 h to remove the adsorbed free PAAM.

The synthesis of PBAM brushes on silicon wafers

The wafers with initiator monolayer were put into 1×10^{-5} m^3 of a DMF solution of 4.47 g (3.14×10^{-2} mol) of Butyl methacrylate, 0.052 g (2.86×10^{-4} mol) of DL-ethyl-bromopropionate (free initiator), 0.098 g (6.0×10^{-4} mol) of 2,2′-bipyridine and 0.030 g (2.9×10^{-4} mol) of CuCl. Under the protection of N_2, the reaction solution was heated at 60 °C for several hours. After the polymerization, the wafers were ultrasonically cleaned for 5 min in DMF and absolute ethanol, and then dried in N_2 stream.

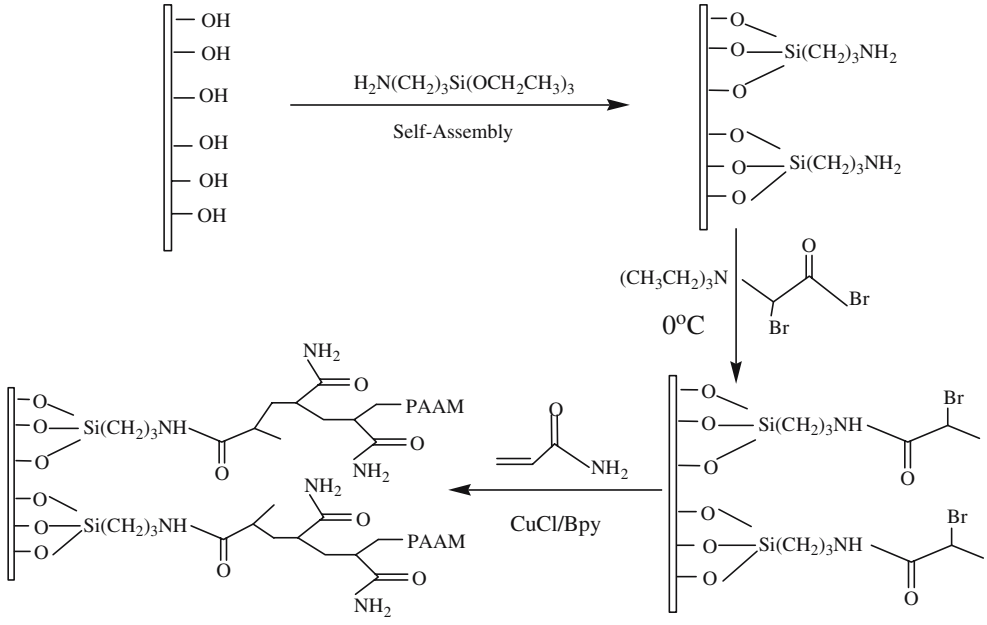

Scheme 2 Synthesis route of PAAM brushes on silicon wafer surface

The synthesis of MMC brushes of PAAM

The PAAM brushes were put into a DMF solution of Pb^{2+} ions for 24 h without stirring at room temperature, and then cleaned with DMF and dried in a N_2 stream, finally PAAM–Pb^{2+} complex brushes were obtained. The procedures for the synthesis of PAAM–Cd^{2+} complex brushes were the same as those of PAAM–Pb^{2+} complex brushes.

Instruments

The X-ray photoelectron spectrum (XPS) was recorded on a VG Scientific ESCA LAB MK II x-probe spectrometer with a monochromatic Mg Ka X-ray source (E_{exc} = 1,256.3 eV) and a hemispherical analyzer at a pass energy of 50 eV to characterize the surface composition of the functionalized silicon wafer and the surface-grafted polymer and MMC brushes. The base pressure during acquisition of the XPS spectra was controlled in the range of 10^{-8}–10^{-9} mbar, and the spot size was 2×7 mm^2. All of the binding energy at the emission angle of the photoelectron at 90° was referenced by setting the CH_x peak at the maximum in the resolved C_{1s} spectra to 285.0 eV. One spectrum was a sum of 5 scans. The measurements were taken at least three times to check the reproducibility. The UV-Visible spectrum (UV) was recorded on a SHIMADZU UV-2450 UV-Visible spectrophotometer. The atomic force microscopy (AFM) observations of the surface were carried out with the commercial instrument (Digital Instrument, Nanoscope IIIa, Multimode). All the tapping mode images were taken at room temperature in air with the microfabricated rectangle crystal silicon cantilevers (Nanosensor). The topography images were obtained at a resonance frequency of approximate 365 kHz for the probe oscillation. The Contact angle measurements of deionized water were performed in air with a Rame-Hart contact angle model 100 goniometry at room temperature. Angles from three different spots on each wafer were measured and statistically compiled.

Results and discussion

In this work, α-bromoester group was selected as a functional group capable of initiating ATRP on the surface of the silicon wafer. A uniform and densely packed initiator-modified substrate was prepared by self-assembly of 3-aminopropyltriethoxysilane, followed by amidation with α-bromopropionyl bromide. In the process of the amidation, triethylamine was used as the catalyst and absorbed HBr from the solution to generate a precipitate of quaternary ammonium halide $(CH_3CH_2)_3NH^+Br^-$, which benefited the amidation. Subsequently the wafers were washed in dry toluene and absolute ethanol in order to remove the free reagents and the absorbed precipitate from the substrate. The contact angle of water on the initiator monolayer was 84.7°, which was significantly different from that of the silicon wafer (15°) before the treatment. It indicated that the properties of the surface were changed due to the addition of a new initiator monolayer.

XPS was used to confirm the formation of the initiator monolayer. The Br 3d peak was observed around 70 eV in the XPS spectrum of the initiator-modified substrate, indicating further the formation of the initiator monolayer. AFM presented a typical topography image of the initiator monolayer (Fig. 8a). A uniform and densely packed surface whose surface roughness was about 0.3 nm could be found, which was used to form the polymer brushes of PAAM and PBMA.

Monomer AAM was chosen to obtain MMC brushes; this is due to AAM containing the nitrogen and oxygen atoms with a lone-pair of electrons which could coordinate to metal ions. According to the previous reports by Wirth and coworkers [23–25], ATRP had been successfully used in the formation of the PAAM brushes grown from solid substrate surface based on the CuCl/bpy catalyst system. Although the detailed proof for the controlled character of ATRP was not provided, researchers were still able to prepare homopolymer brushes and block copolymer brushes of AAM by surface-initiated ATRP method. On the basis of the above reason, we chose AAM as the monomer to prepare the MMC brushes.

During the course of polymerization, DMF was used as the solvent for the polymerization of AAM, as the initiator was attached to the silicon wafers, ATRP of AAM on the silicon wafer was out of phase. According to the polymerization conditions carried out in previous reports [23–25], no deactivator or 'sacrificial' initiator were added into the reaction. Two piece of silicon wafers, one of which was covered with initiator, the other was blank, were put into the reaction solution. Reaction temperature was high (120 °C) enough to lead to the thermal polymerization of AAM, however, the catalyst and a large amount of monomer AAM remained in the reaction solution, the polymerization carried out on the surface of the wafers still continued. After the polymerization, on the blank wafer no PAAM brushes were found, which indicated the free PAAM in the solution did not adhere to the

surface, so the PAAM brushes were formed on the silicon wafer only by ATRP technique. The PAAM brushes attached to the silicon wafers were immersed into a large amount of ultrapure water for 24 h to remove the adsorbed PAAM. Thus, the surface of the brushes could be observed actually by AFM, otherwise, the absorbed PAAM would have an influence on the surface topography image.

Figure 1 showed typical UV–Visible absorption spectra of the initiator monolayer before (a) and after (b) the polymerization of AAM. From the comparison of the absorption spectrum of the initiator monolayer with that of the PAAM brushes, it could be found that an obvious absorption of PAAM brushes appeared, which was caused by the C=O of the repeat unit of the PAAM brushes, confirming the existence of PAAM brushes on the silicon wafers.

XPS was used to characterize the surface of the polymer brushes. Two peaks of the Si 2p electrons were found before and after the polymerization at 102.5 eV and 98.9 eV, which were assigned to the SiO_2 and silicon, respectively. After the polymerization, the decrease of the intensity of the two peaks indicated the addition of the organic polymer to the surface (Fig. 2). Simultaneously, the increase of the intensity of the silicon peak (98.9 eV) relative to that of the SiO_2 peak (102.5 eV) could be caused by the deoxidization of SiO_2 during ATRP.

Besides the Si 2p peaks, the C 1s peak appeared around 285 eV with a broad shoulder at the higher binding energy. According to the references [26], the high resolution region of the XPS spectra of the C 1s was fitted with multiple Gaussians, there were three peaks representing three different carbons (Fig. 3) in homopolymer PAAM brushes: (1) aliphatic hydrocarbon (C–C at 284.7 eV); (2) an amide induced β-shifted carbon (C–$CONH_2$ at 285.7 eV); (3) the amide carbon ($CONH_2$ at 288.1 eV). The contact angle of water on hydrophilic PAAM brushes was 17.1°, which showed obviously hydrophilicity and was different from that of initiator monolayer on the wafer (84.7°). Moreover, the XPS quantitative analysis for the PAAM brushes gave rise to a molar ratio of 2.80C:1.00O:0.75N, in good

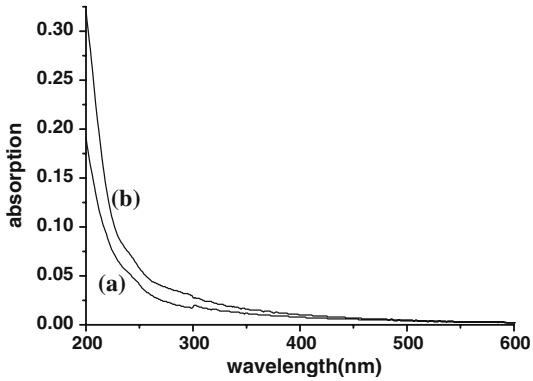

Fig. 1 The UV–visible absorption spectra of initiator monolayer (**a**) and PAAM brushes (**b**) on quartz slide

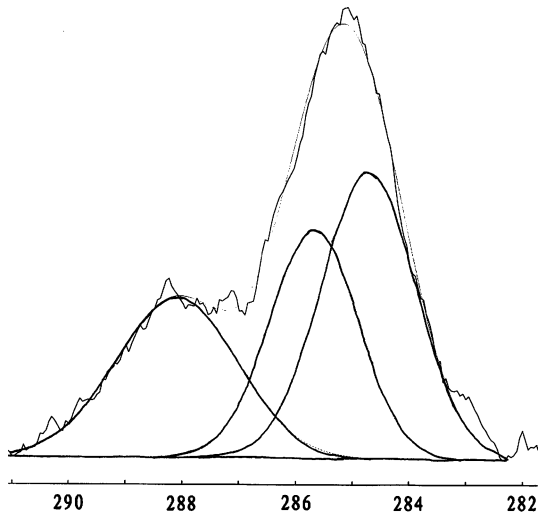

Fig. 3 The C 1s XPS spectra of PAAM homopolymer brushes on silicon wafer

Fig. 2 The peak of Si 2p in XPS spectra of initiator monolayer (**a**) before the polymerization and PAAM brushes (**b**) after the polymerization

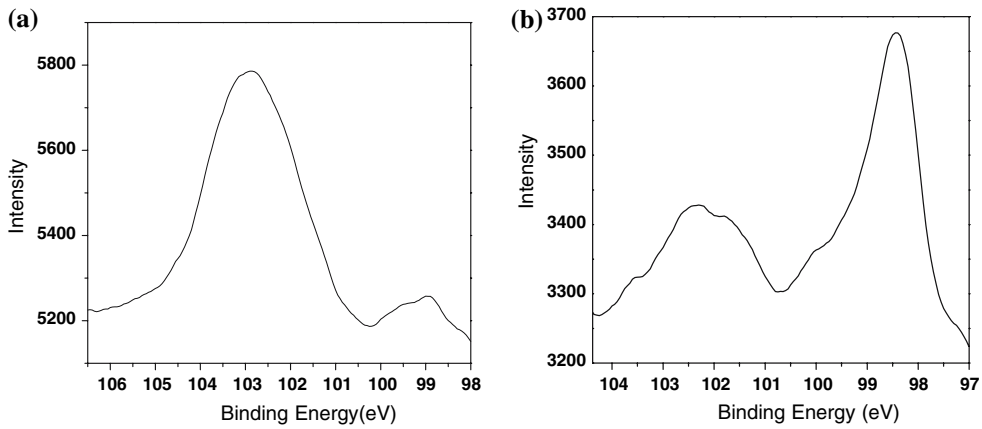

agreement with the value (a molar ratio of 3.00C:1.00O:1.00N) based on the monomer AAM [27]. All these effects suggested the attachment of the PAAM brushes onto the surface of the silicon wafer.

Figure 4 showed the surface morphologies of PBMA and PAAM brushes for comparison. A uniform PBMA brushes were found, however, on the height images of the PAAM brushes nanoscale protrusions whose mean diameter was about 50 nm were clearly visible, moreover, could not be detected on the initiator monolayer prior to the polymerization (Fig. 8a). From the AFM topography images it could be observed that the mean thickness of PAAM and PBMA brushes through imaging across the scratch boundary [28] were 30 nm and 35 nm, respectively, which had exceeded the escape depth of photoelectrons (about 11 nm [29]). As the surface of the initiator-modified substrate was uniform, the silicon wafers were covered with PAAM brushes and PBMA brushes completely; however, the silicon signal was still detected in PAAM brushes but not detected in PBMA brushes by mean of XPS. The XPS spectra of the PAAM layers exhibited a weak silicon signal, indicating that in some domains the thickness of the polymer layer was not larger than the escape depth of the photoelectrons. It suggested that the nanoscale protrusions of PAAM should be formed on silicon wafers. As one possibility, thermal polymerization of AAM enabled the reaction solution more viscous, the tethered PAAM chains hardly stretched out enough in the mixture solution, gathering together and twisting with one another, which prevented the propagating of some active PAAM chains; secondly, it was caused by the uncontrolled character during ATRP of AAM based on the CuCl/bpy catalyst. Unfortunately, the amount of the polymer brushes bound to the silicon wafer was extremely small, we were not able to determine the molecular weight, the polydispersity and the degree of polymerization by cleaving them from the substrate; however, this did not deny the nature of the ATRP technique, which had been approved in pioneering experiments [23–25].

As a polymer ligand containing anchoring sites, PAAM brushes with a lot of nanoscale protrusions were used to synthesize MMC brushes of metal ions, Pb^{2+} and Cd^{2+}, based on the formation of the coordinate bonds.

In the XPS spectrum of PAAM–Pb^{2+} complex brushes linking to the silicon wafer surface, the occurrence of new peaks at 139.1 eV and 143.8 eV, originating from coordinated Pb($4f_{7/2}$) and Pb($4f_{5/2}$), respectively, verified the existence of Pb^{2+} ions (Fig. 5a). For PAAM–Cd^{2+} complex brushes, two new peaks of coordinated Cd 3d electrons were detected at 405.4 eV ($3d_{5/2}$) and 412.5 eV ($3d_{3/2}$), respectively (Fig. 5b). From the occurrence of the new signals of metal ions, it was obvious that the MMC brushes of PAAM had been prepared. Besides the metal ions peaks, the Si peak of the MMC brushes was still detected, which suggested that the introduction of the metal ions did not change the morphology of the brushes, the nanoprotrusions still existed on the surface of the MMC brushes.

The XPS measurements were carried out to obtain much more insight into the information on the structures of the MMC brushes, based on the variance of the binding energies of the elements such as O_{1s} and N_{1s} of the $–CONH_2$ group. The XPS assignments are summarized in Table 1. It was obvious that metal–ligand (PAAM) coordination increased the binding energies of N_{1s} and O_{1s} electrons in the $–CONH_2$ groups, which was ascribed to the reason that the 2p electrons binding energies of nitrogen and oxygen might be perturbed upon coordination to metal ions. For PAAM brushes, in the N_{1s} region (Fig. 6b) there was one peak at 399.9 eV caused by the N atom of the $–CONH_2$ group.

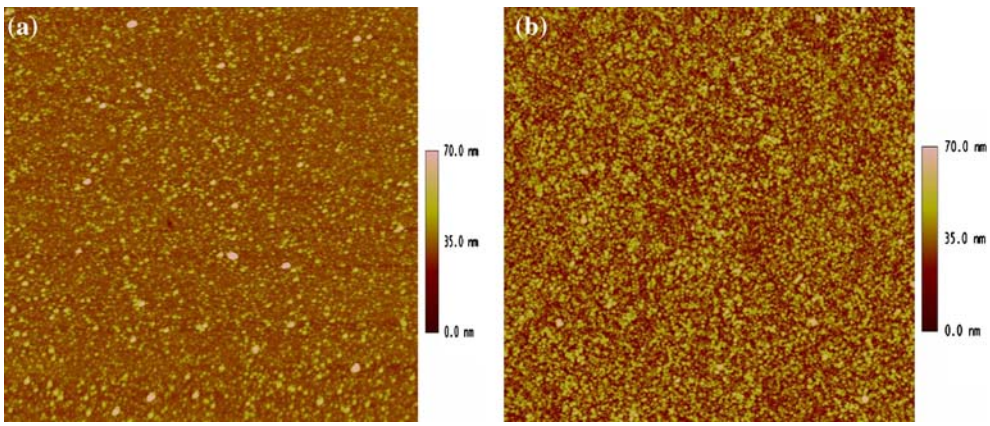

Fig. 4 AFM images of PAAM homopolymer brushes (**a**) and PBMA homopolymer brushes (**b**). The state of AFM: Scan size: 10 μm; Scan rate: 1.026 HZ; Image Date: Height; Date Scale: 70.00 nm

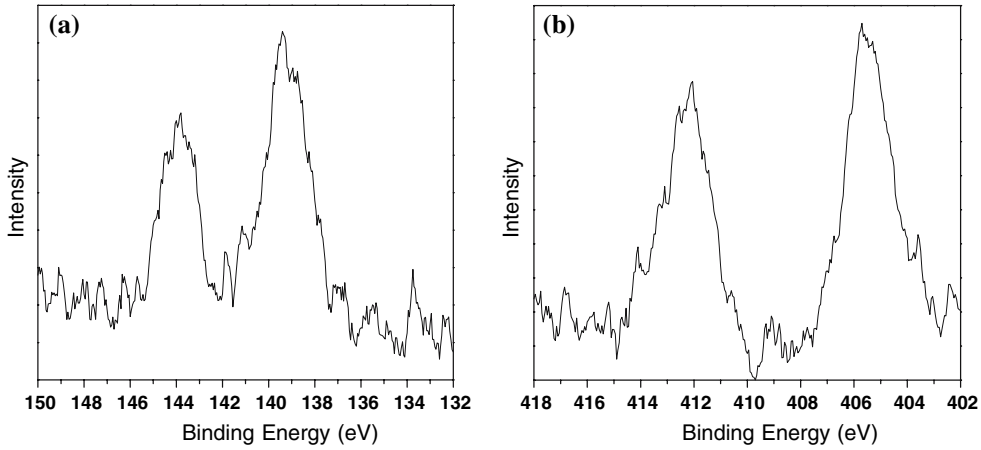

Fig. 5 The peaks of coordinated Pb_{4f} (**a**) and Cd_{3d} (**b**) in XPS spectrum of MMC brushes

Table 1 Binding energies (eV) and composition for XPS spectra of PAAM brushes and MMC brushes[a]

Assignment	PAAM	MMC (Pb^{2+})	MMC (Cd^{2+})
O1s	531.8	532.3	531.8
N1s	399.9	400.2	400.1
$Pb^{2+}{}_{4f}$	–	139.1, 143.8	–
$Cd^{2+}{}_{3d}$	–	–	405.4, 412.5

[a] It was assumed that the $-CONH_2$ groups detected by the photoelectrons of XPS all participated in coordination with metal ions

In the O_{1s} region (Fig. 7b), the peak at 531.8 eV was assigned to the carboxyl oxygen. With the introduction of metal cations, an increase of 0.2 eV and 0.3 eV for the N_{1s} signals in XPS spectrum (Fig. 6) was consistent with Cd^{2+} and Pb^{2+} coordination to the AAM nitrogen lone pair, respectively. At the same time, it could be seen that the peak corresponding to O_{1s} electrons exhibited an increase of 0.5 eV due to Pb^{2+} coordination to the carbonyl oxygens. However, the O_{1s} peak seemed not to be influenced by the coordination of Cd^{2+} ions (Fig. 7), which suggested two possibilities: on the one hand, the quantity of the oxygen atoms participating in coordination was too few to detect the shift of the peak; on the other hand, the coordinate bond between O atoms and Cd^{2+} ions was weak enough not to affect the binding energies of O_{1s} electrons. The variance of their binding energies suggested that both O atoms and N atoms participated in coordination in the PAAM–Pb^{2+} complex, however, the anchoring sites of the PAAM–Cd^{2+} complex were mainly nitrogen atoms. While from the comparison with the shift of the binding energies of N_{1s}, we could see that the variance of the binding energies in the PAAM–Cd^{2+} complex brushes was smaller than that in the PAAM–Pb^{2+} complex brushes, which indicated a stronger coordinate bond between N and Pb^{2+}. According to the above data, it was clear that the MMC brushes of Pb^{2+} and Cd^{2+} with different structures had been prepared.

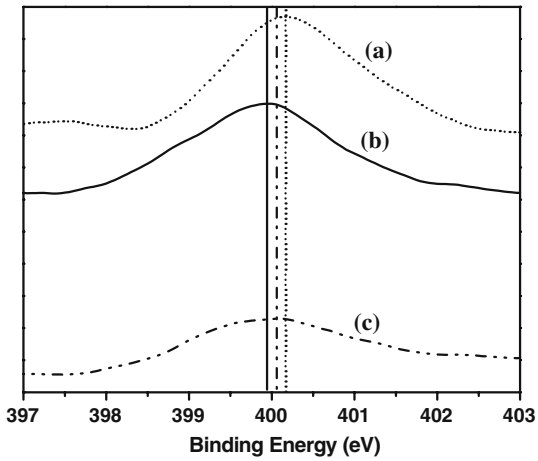

Fig. 6 The peak of N_{1s} in XPS spectra of MMC–Pb^{2+} brushes (**a**), PAAM brushes (**b**), MMC–Cd^{2+} brushes (**c**)

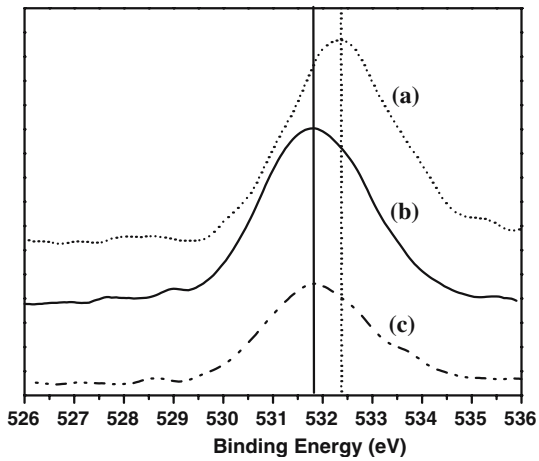

Fig. 7 The peak of O_{1s} in XPS spectra of MMC–Pb^{2+} brushes (**a**), PAAM brushes (**b**), MMC–Cd^{2+} brushes (**c**)

Simultaneously, AFM was used to characterize the surface of the MMC brushes, it was observed that nanoscale protrusions were still distributed uniformly over the surface. To clarify the variances of the surface topography, the height images of the initiator monolayer, PAAM brushes and the MMC brushes were shown in Fig. 8 By taking cross section through the AFM height images, the evaluation of their size and the area density could also be performed. As shown in Fig. 8a, the initiator monolayer was uniform.

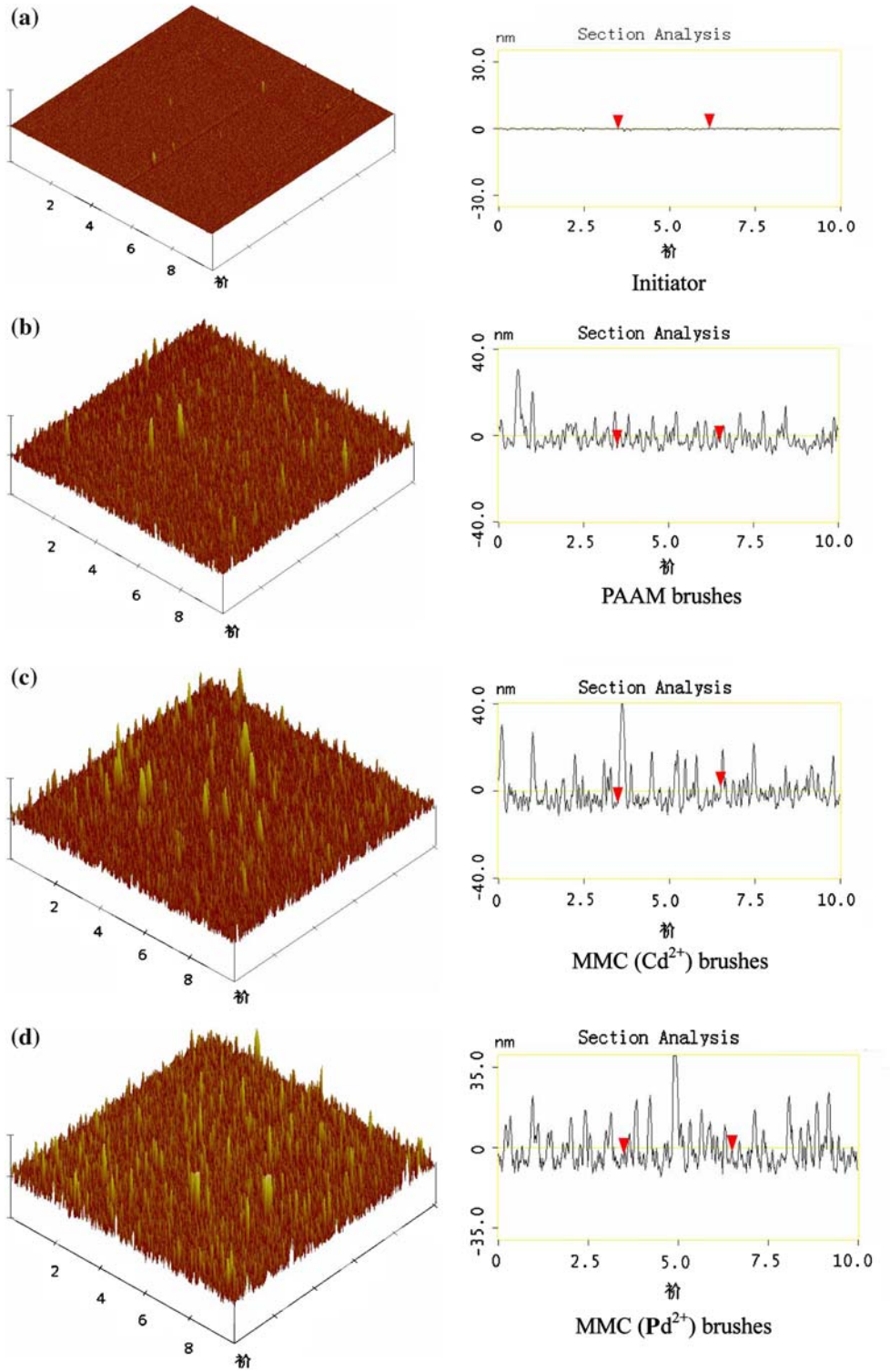

Fig. 8 Three-dimensional height images and the cross section of (**a**) Initiator; (**b**) PAAM brushes; (**c**) MMC (Cd^{2+}) brushes; (**d**) MMC (Pb^{2+}) brushes. The state of AFM: Scan size: 10 μm; Scan rate: 1.026 HZ; Image Date: Height; Date Scale: 70.00 nm

From the PAAM brushes (Fig. 8b) to the MMC brushes (Fig. 8c, d), the size of the nanoscale protrusions obviously increased wherever these observations were reproducible on the surface, while the area density of the protrusions decreased. According to the variance of the surface roughness, we could obtain the same results as the above, it was clear that the surface roughness increased from 5.3 ± 0.2 nm (PAAM brushes) to 7.0 ± 0.4 nm (MMC–Cd^{2+} brushes) and to 8.00 ± 0.4 nm (MMC–Pb^{2+} brushes) with the introduction of the metal ions. As the anchoring sites nitrogen and oxygen atoms were rich in the outer surface of the nanoscale protrusions of PAAM brushes, when PAAM brushes were put into the solution of metal ions, By accumulating the polymer chains due to metal ions bridging among the PAAM nanoprotrusions by a coordinate bond and the overlap of neighboring nanoprotrusions, an increase of the size of a protrusions and a slight decrease of the number of protrusions were found, thus, metal ions were not only distributed uniformly over the surface of the nanoprotrusions, but also existed in the inner of the nanoprotrusions.

Comparing the three-dimensional height images and the cross section of the MMC brushes, we could observe that the size of nanoprotrusions of MMC–Pb^{2+} brushes was larger than that of MMC–Cd^{2+} brushes, at the same time, the difference between the surface roughnesses also verified this result. A possible reason was that the coordination capabilities of PAAM ligand to two kinds of metal ions were different. In MMC–Pb^{2+} brushes a strong coordinate bond was formed between Pb^{2+} ions and the N and O atoms, however, in MMC–Cd^{2+} brushes only the N atoms possessed a relatively weak coordination ability to Cd^{2+} ions, once the metal ions Pb^{2+} were introduced into the PAAM systems, relative to Cd^{2+} ions, leading to the overlap of the more neighboring nanoprotrusions, the larger size nanoprotrusions on the surface of MMC–Pb^{2+} brushes were formed. Based on the above analysis, the results of the topography image by AFM were in agreement with that of the XPS spectra.

Conclusions

By combining the self-assembly of initiator, ATRP and coordination to metal ions, Pb^{2+} and Cd^{2+}, PBMA and PAAM homopolymer brushes and the functional MMC brushes of PAAM were prepared on the surface of silicon wafers. The formation of the initiator monolayer, PAAM brushes and the MMC brushes was confirmed by XPS and contact angle measurement. AFM was used to characterize the surface of the initiator monolayer, PBMA brushes, PAAM brushes and the MMC brushes of PAAM, the surfaces of the initiator monolayer and PBMA brushes were uniform, however, the nanoprotrusions were found on the surface of PAAM brushes, moreover, introduction of metal ions into PAAM brushes induced an increase of the size of the protrusions by accumulating the polymer chains, while a slight decrease of the number of the protrusions might be due to the overlap of the neighboring protrusions. From AFM images, it was obvious that the size of nanoprotrusions of MMC–Pb^{2+} brushes was larger than that of MMC–Cd^{2+} brushes due to the difference of the coordination capabilities of metal ions. We do believe that this study opens up a new avenue. After the suitable modification of MMC brushes, these polymers should have interesting properties for many applications, such as electrochemical materials, optimized sensory, etc.

In addition, experiments aiming at controlling the size of nanoscale protrusions of PAAM brushes and further controlling the size of the MMC nanoprotrusions by altering the reaction conditions according to this method are currently under way. The MMC brushes are rich of metal ions, Cd^{2+} and Pb^{2+}, once the reaction of them with H_2S gas takes place, it is possible that PbS and CdS nanoparticles on/in the films be synthesized to form a new kind of organic/inorganic nanoparticles/polymer materials [30], not only inorganic PbS or CdS nanoparticles but also macromolecules nanoprotrusions exist in this systems, which will be reported elsewhere.

References

1. Milner ST (1991) Science 251:905
2. Xu FJ, Yuan ZL, Kang ET, Neoh KG (2004) Langmuir 20:8200
3. Zhao B, Brittain WJ (2000) Prog Polym Sci 25:677
4. Mori H, Müller AHE (2003) Top Curr Chem 228:1
5. Hierlemann A, Campbell JK, Baker LA, Crooks RM, Ricco AJ (1998) J Am Chem Soc 120:5323
6. Tully DC, Trimble AR, Fréchet JMJ, Wilder K, Quate CF (1999) Chem Mater 11:2892
7. Li J, Piehler LT, Qin D, Baker JR, Tomalia DA, Meier DJ (2000) Langmuir 16:5613
8. Zhao B, Zhu L (2006) J Am Chem Soc 128:4574
9. Xu FJ, Song Y, Cheng ZP, Zhu XL, Zhu CX, Kang ET, Neoh KG (2005) Macromolecules 38:6254
10. Li C, Benicewicz BC (2005) Macromolecules 38:5929
11. Senaratne W, Andruzzi L, Ober CK (2005) Biomacromolecules 6:2427
12. Fan X, Lin L, Dalsin JL, Messersmith PB (2005) J Am Chem Soc 127:12843
13. Bontempo D, Tirelli N, Feldman K, Masci G, Crescenzi V, Hubbell JA (2002) Adv Mater 14:1239

14. Pyun J, Kowalewski T, Matyjaszewski K (2003) Macromol Rapid Commun 24:1043
15. Coessens V, Pinrauer T, Matyjaszewski K (2001) Prog Polym Sci 26:337
16. Matyjaszewski K, Xia J (2001) Chem Rev 101:2921
17. Kaliyappan T, Kannan P (2000) Prog Polym Sci 25:343
18. Rivas BL, Seguel GV (2000) Polym Bull 44:445
19. Basova YV (2001) J Solid State Eelectrochem 5:512
20. Das P, Indra EM, Belfiore LA (1997) Polym Eng Sci 37:1909
21. Koutsos V, van der Vegte EW, Hadziioannou G (1999) Macromolecules 32:1233
22. Kong X, Kawai T, Abe J, Iyoda T (2001) Macromolecules 34:1837
23. Huang X, Wirth MJ (1997) Anal Chem 69:4577
24. Huang X, Doneski LJ, Wirth MJ (1998) Anal Chem 70:4023
25. Xiao D, Wirth MJ (2002) Macromolecules 35:2919
26. Watts JF, Leadley SR, Castle JE, Blomfield CJ (2000) Langmuir 16:2292
27. Wang J, Chen W, Liu A, Lu G, Zhang G, Zhang J, Yang B (2002) J Am Chem Soc 124:13358
28. Jones DM, Huck WTS (2001) Adv Mater 13:1256
29. Chen X, Gardella JA, Kumler PL (1993) Macromolecules 26:3778
30. Jiang P, Liu Z, Cai S (2002) Langmuir 18:4495